Available online at www.sciencedirect.com
SCIENCE DIRECT®
Applied Surface Science 248 (2005) 433–439
applied surface science
www.elsevier.com/locate/apsusc

Channels of energy redistribution in short-pulse laser interactions with metal targets

Leonid V. Zhigilei *, Dmitriy S. Ivanov [1]

Department of Materials Science and Engineering, University of Virginia, 116 Engineer's Way, Charlottesville, VA 22904-4745, USA

Available online 30 March 2005

Abstract

The kinetics and channels of laser energy redistribution in a target irradiated by a short, 1 ps, laser pulse is investigated in computer simulations performed with a model that combines molecular dynamics (MD) simulations with a continuum description of the laser excitation and relaxation of the conduction band electrons, based on the two-temperature model (TTM). The energy transferred from the excited electrons to the lattice splits into several parts, namely the energy of the thermal motion of the atoms, the energy of collective atomic motions associated with the relaxation of laser-induced stresses, the energy carried away from the surface region of the target by a stress wave, the energy of quasi-static anisotropic stresses, and, at laser fluences above the melting threshold, the energy transferred to the latent heat of melting and then released upon recrystallization. The presence of the non-thermal channels of energy redistribution (stress wave and quasi-static stresses), not accounted for in the conventional TTM model, can have important implications for interpretation of experimental results on the kinetics of thermal and mechanical relaxation of a target irradiated by a short laser pulse as well as on the characteristics of laser-induced phase transformations. The fraction of the non-thermal energy in the total laser energy partitioning increases with increasing laser fluence.

PACS: 61.80.Az; 79.20.Ds; 02.70.Ns; 64.70.Dv

Keywords: Laser interactions; Molecular dynamics; Laser energy redistribution; Laser melting; Heat transfer; Laser-induced stresses

1. Introduction

Short-pulse laser irradiation of a metal target triggers a cascade of processes involved in the energy redistribution between the energy of the conduction band electrons that absorb the laser irradiation and energy of the thermal and collective atomic motions.

* Corresponding author. Tel.: +1 434 243 3582; fax: +1 434 982 5660.
E-mail addresses: lz2n@virginia.edu (L.V. Zhigilei), dmitriy@nuigalway.ie (D.S. Ivanov).
[1] Present address: National Centre for Laser Applications, Galway, Ireland.

0169-4332/$ – see front matter © 2005 Elsevier B.V. All rights reserved.
doi:10.1016/j.apsusc.2005.03.062

The processes of energy redistribution include the ballistic energy transport by the excited electrons, the electronic heat diffusion, the energy transfer from electrons to the atomic vibrations due to the electron–phonon coupling, the energy transfer by acoustic waves emitted from the absorption region, and the transformation of the deposited laser energy to the energy of phase transitions or other structural changes occurring in the target material due to the laser-induced heating and stresses. The purpose of the computational study reported in this paper is to explore the relative importance of different channels of the energy redistribution in a metal target irradiated by a short laser pulse.

Computational modeling of short-pulse laser interaction with metals is commonly based on the so-called two-temperature model (TTM) [1], which describes the time evolution of the lattice and electron temperatures, T_l and T_e, by two coupled non-linear differential equations. The model accounts for the laser excitation of the conduction band electrons, energy transfer to the atomic vibrations due to the electron–phonon coupling, and the electronic heat diffusion from the irradiated surface to the bulk of the target. Despite numerous successful applications of TTM, e.g. [2–5], the inherent limitation of the model is its inability to describe a number of important non-diffusive energy transfer and transformation channels that may have a strong effect on the temperature evolution in the target and on the final outcome of short-pulse laser irradiation.

Some of the non-diffusive energy transfer processes can be accounted for by updating TTM with additional capabilities. In particular, a description of the initial energy transfer by ballistic electrons in s/p-band metals, where electron–electron collision rate is relatively small and the mean free path of the excited electrons can be significantly larger than the optical absorption depth, should be added to the conventional TTM [2,6]. The generation of thermoelastic stresses and the emission of the acoustic waves from the surface region of the irradiated target are important processes that can be accounted for by combining TTM (or the common thermal diffusion equation at later times, when electron–phonon equilibrium has been established) with thermoelasticity equations [7].

While the processes mentioned above can be described at the continuum level, within the framework provided by TTM, computational description of laser-induced phase transformations and changes in the microstructure is much more challenging. The mechanisms and kinetics of fast phase transformations and damage occurring under highly non-equilibrium conditions induced in the target material by short-pulse laser irradiation are not well understood and, therefore, cannot be reliably described at the continuum level, by a set of kinetic equations.

In order to overcome the limitations of TTM, we have recently developed a combined atomistic-continuum model capable of a realistic description of laser-induced structural transformations [8]. The model incorporates the classical molecular dynamics (MD) method for simulation of non-equilibrium processes in the surface region of irradiated target into the general framework of the TTM model. First applications of the combined TTM–MD model have provided insights into the microscopic mechanisms of laser melting and photomechanical damage in metal films and bulk targets [8–13]. In this paper, we perform a detailed analysis of the kinetics and channels of laser energy redistribution in two representative simulations performed for bulk Ni targets. The first simulation is done in thermoelastic regime, at a laser fluence below the threshold for laser melting. The second simulation is performed above the melting threshold, when melting and resolidification processes affect the redistribution of the energy deposited by the laser pulse, but below the threshold for photomechanical damage or spallation [10]. Comparative analysis of the results of the two simulations provides information on the relative contribution of different laser-induced processes to the energy partitioning and redistribution in the irradiated target. A brief description of the combined TTM–MD model is given in Section 2, followed by the results and conclusions.

2. Computational model

A detailed description of the combined TTM–MD model is given elsewhere [8]. In this section, we only provide a brief discussion of the main features of the model and give the parameters of the simulations presented in this paper. In the TTM–MD model, MD representation of the atomic structure substitutes the

TTM equation for the lattice temperature in the surface region of the irradiated target. The diffusion equation for the electron temperature is solved by a finite difference method simultaneously with MD integration of the equations of motion of atoms. The electron temperature enters a coupling term that is added to the MD equations of motion to account for the energy exchange between the electrons and the lattice. The cells in the finite difference discretization are related to the corresponding volumes of the MD system and the local lattice temperature is calculated for each cell from the average kinetic energy of the thermal motion of atoms. The expansion, density variations, and, at higher fluences, disintegration of the surface region of the target predicted in the MD part of the model are accounted for in the continuum part of the model.

The MD method is used only in the surface region of the target, where active processes of laser melting, spallation, and ablation are taking place, whereas the diffusion equation for the electron temperature is solved in a much wider region affected by the thermal conduction. A special pressure-transmitting boundary condition [14,15] is used to simulate the propagation of the laser-induced pressure wave from the surface region of the target represented by the MD method to the continuum part of the model. The energy carried away by the wave is monitored, allowing for control over the total energy conservation in the combined model. In the continuum part of the model, beyond the MD region, the energy exchange between the electrons and the lattice is described by the conventional TTM, in which the phonon contribution to the heat conduction is neglected. The temperature dependence of the lattice heat capacity, obtained for the model material, is approximated by a polynomial function and is used in the TTM equation for the lattice temperature.

The thermal and elastic properties of the lattice, such as the lattice heat capacity, elastic moduli, coefficient of thermal expansion, melting temperature, volume, and entropy of melting and vaporization, etc., are all defined by the interatomic interaction, described in this work by the embedded-atom method (EAM) in the form suggested in Ref. [16]. Some of the parameters of the model EAM Ni material are reported in [8,13]. The parameters used in the TTM equation for the electron temperature are listed below. The electronic heat capacity is $C_e = AT_e$ with $A = 1065\ \mathrm{J\ m^{-3}\ K^{-2}}$, the thermal conductivity is $K_e = K_0 T_e/T_l$ with $K_0 = 91\ \mathrm{W\ m^{-1}\ K^{-1}}$, the electron–phonon coupling constant $G = 3.6 \times 10^{17}\ \mathrm{W\ m^{-3}\ K^{-1}}$ and the optical absorption depth is $L_p = 13.5$ nm.

The initial MD system used in the simulations reported in this work is an FCC crystal composed of 113,200 atoms with dimensions of 3.53 nm × 3.53 nm × 99.94 nm and periodic boundary conditions imposed in the directions parallel to the (1 0 0) free surface. The continuum part of the combined TTM–MD model extends by 900 nm beyond the back end of the MD computational cell, providing an adequate representation of the electronic heat conduction into the bulk of the target. The system is equilibrated at 300 K before applying laser irradiation.

3. Results and discussion

Simulations discussed in this paper are performed at two absorbed fluences, 21.5 and 107.5 mJ/cm^2, with laser pulses of Gaussian temporal profile and pulse duration (defined as full width at half maximum) of

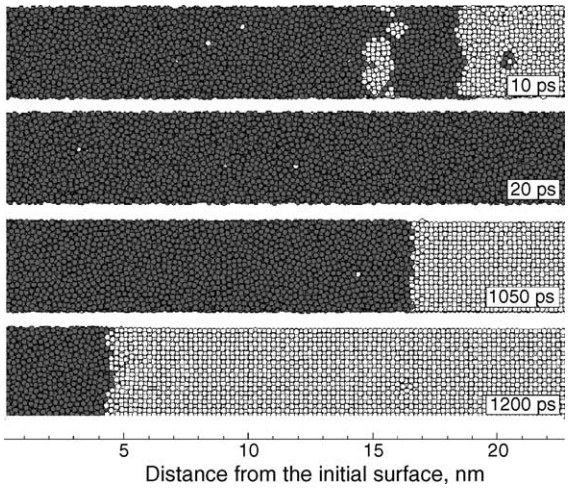

Fig. 1. Snapshots from a simulation of laser melting and recrystallization of a surface region of a Ni target irradiated with a 1 ps laser pulse at an absorbed fluence of 107.5 mJ/cm^2. Atoms are colored according to the local order parameter [8]–white atoms have local crystalline surroundings, dark atoms belong to the liquid phase. Snapshots taken at 10 and 20 ps after the laser pulse illustrate the process of fast homogeneous melting of the sub-surface region. Snapshots taken at 1050 and 1200 ps show epitaxial recrystallization of the region.

1 ps. A qualitative picture of the laser-induced processes can be obtained from a mere visual inspection of snapshots of atomic-level structure in the surface regions of the irradiated targets. In the case of 21.5 mJ/cm^2, the material response to laser irradiation is limited to thermoelastic motion of the crystalline target, with no melted regions observed. At 107.5 mJ/cm^2, however, we observe melting of 61 nm surface region of the target followed by recrystallization, as illustrated by Fig. 1. Two stages can be identified in the melting process, an ultrafast melting of 56 nm region of the target within 35 ps, followed by a slower expansion of the melted region by 5 nm within about 200 ps. A similar two-stage melting process with a fast (5–10 ps) and a slow (hundreds of ps) components has been deduced from time-resolved reflectivity measurements performed for thermal melting of GaAs irradiated by a 100 fs laser pulse [17]. We find that the fast melting component corresponds to the homogeneous nucleation and growth of liquid regions inside the overheated crystal (e.g., snapshot taken at 10 ps in Fig. 1), whereas the slower melting component corresponds to heterogeneous melting that proceeds by the propagation of the liquid–crystal interface. A two-stage melting process has been also observed in our earlier simulations performed for thin metal films [8,9]. Starting from about 250 ps after the laser pulse a reverse process of epitaxial recrystallization starts and results in the complete recrystallization of the transiently melted region of the target by the time of 1300 ps after the laser pulse. Advancement of the crystallization front towards the surface can be seen in the snapshots taken at 1050 and 1200 ps in Fig. 1.

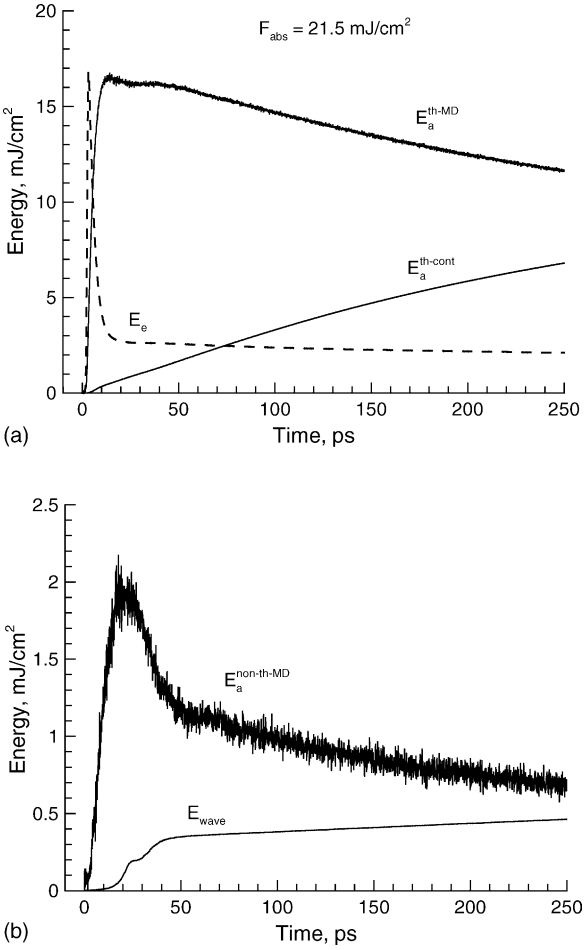

Fig. 2. Energy redistribution in a Ni target irradiated with a 1 ps laser pulse at an absorbed fluence of 21.5 mJ/cm^2. The thermal energy of the electrons, E_e, along with the thermal energies of the atoms in the MD part (top 100 nm) and the continuum part (next 900 nm) of the TTM–MD computational cell, $E_a^{th\text{-}MD}$ and $E_a^{th\text{-}cont}$, respectively, are shown in (a). The energy removed from the MD part of the computational cell by the outgoing stress wave, E_{wave}, and the non-thermal energy associated with collective atomic motions and quasi-static anisotropic thermoelastic stresses, $E_a^{non\text{-}th\text{-}MD}$, are shown in (b). The thermal energies in (a) are shown relatively to their values before the irradiation, in the target equilibrated at 300 K.

The kinetics and channels of laser energy redistribution in the two simulations briefly discussed above are illustrated in Figs. 2 and 3. We start from the analysis of the simulation performed at the lower fluence of 21.5 mJ/cm^2, in which no melting is observed. The total energy deposited by the laser is equal to the absorbed laser fluence and is conserved after the end of the laser pulse for the rest of the simulation. Initially, during the laser pulse, all the energy is deposited into the thermal energy of the electrons, E_e (Fig. 2a). Strong electron–phonon coupling in Ni results in the fast, within ~15 ps, energy transfer to the thermal energy of atomic motions. Part of the energy is transferred from the electrons to the lattice during the laser pulse and the maximum energy of the electrons in Fig. 2a does not reach the value of the absorbed laser fluence, 21.5 mJ/cm^2. The initial depth of the surface layer heated by the laser pulse is defined by the penetration depth of the excited electrons before the electron–phonon equilibration, L_c, that has been estimated for Ni to be ~50 nm [12]. Therefore, the initial increase of the thermal energy of atomic motions

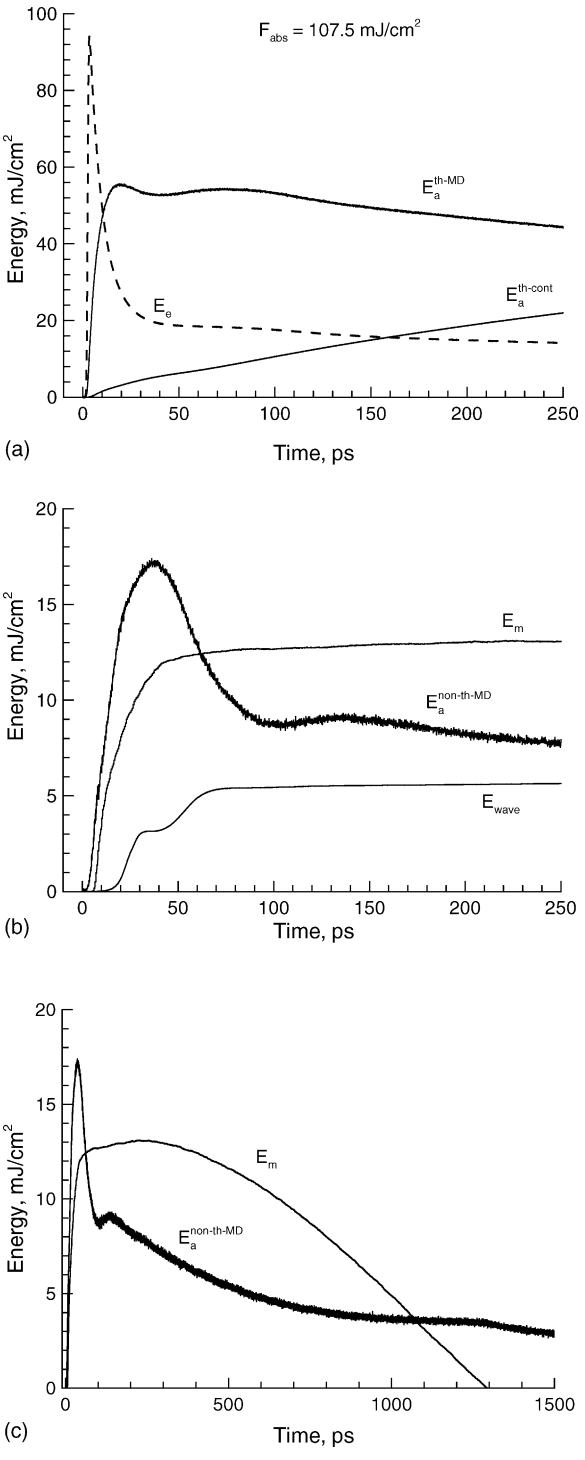

Fig. 3. Energy redistribution in a Ni target irradiated with a 1 ps laser pulse at an absorbed fluence of 107.5 mJ/cm^2. All the nomenclature in (a) and (b) is the same as in Fig. 2, with an additional line for the energy that went to the latent heat of melting, E_m, shown in (b). An expanded view for a time range up to 1500 ps after the laser pulse is shown in (c) for $E_a^{non\text{-}th\text{-}MD}$ and E_m. The thermal energies in (a) are shown relatively to their values before the irradiation, in the target equilibrated at 300 K.

can be observed only for the top 100 nm layer of the target represented by MD, $E_a^{th\text{-}MD}$. The thermal energy of atomic motions includes contributions from the kinetic and potential energies of the MD system and is calculated based on the virial theorem [18]. As time progresses, the fast electronic heat conduction leads to the energy transfer from the top 100 nm surface layer to the deeper part of the target represented at the continuum level, as evidenced by the energy flow from $E_a^{th\text{-}MD}$ to $E_a^{th\text{-}cont}$ (Fig. 2a).

Additional channels for partitioning the deposited energy, not accounted for in the conventional TTM but present in a more realistic TTM–MD model, are shown in Fig. 2b. The fast transfer of more than half of the deposited laser energy to the thermal energy of atomic motions, $E_a^{th\text{-}MD}$, takes place under conditions of inertial stress confinement [10] and leads to the buildup of the compressive stresses in the surface region of the irradiated target. The initial stresses relax by driving a strong compression wave into the bulk of the target, followed by a tensile component of the wave that results from the interaction of the compressive stresses with the free surface of the target. The energy carried away from the MD part of the model (top 100 nm surface region of the target) by the outgoing stress wave, E_{wave}, is shown as a function of time in Fig. 2b. Two-step increase of E_{wave} can be attributed to the consecutive propagation of the compressive and tensile components of the bimodal thermoelastic wave through the non-reflecting boundary at the bottom of the MD part of the combined atomistic-continuum model.

The relaxation of the laser-induced stresses also results in the transformation of a part of the deposited laser energy into non-thermal energy associated with collective atomic motions as well as quasi-static anisotropic thermoelastic stresses in the surface region of the target represented by MD, $E_a^{non\text{-}th\text{-}MD}$ in Fig. 2b. The collective atomic motions are related to the generation of the stress wave discussed above, whereas the origin of the quasi-static stresses can be explained as follows. For a typical laser spot diameter of ~100 μm, the fast relaxation of the laser-induced stresses can only

proceed in the direction normal to the surface. These conditions of lateral confinement are correctly reproduced by the periodic boundary conditions applied in the simulations in the directions parallel to the surface. The uniaxial expansion of the surface region of the target results in anisotropic lattice deformations and corresponding anisotropic stresses. The residual anisotropic stresses cannot relax by uniaxial expansion and remain in the surface region of the target as long as the temperature of the irradiated surface exceeds the temperature of the bulk of the target. The initial spike of the non-thermal energy, $E_a^{\text{non-th-MD}}$, observed in Fig. 2b during the first 50 ps is related, therefore, to the dynamic relaxation of the thermoelastic stresses and generation of the stress wave, whereas the slowly decreasing component of the non-thermal energy at later times is related to the quasi-static stresses. The energy associated with the quasi-static stresses decreases as the surface region cools down due to the heat conduction to the bulk of the target. The fraction of the total absorbed laser energy transferred into non-thermal energy in both atomistic and continuum parts of the system ($E_a^{\text{non-th-MD}} + E_{\text{wave}}$) changes from ~10% at the peak of the dynamic relaxation of thermoelastic stresses at ~25 ps, to ~5% at 250 ps after the laser pulse.

The overall picture of the energy redistribution in a simulation performed at a higher absorbed fluence of 107.5 mJ/cm^2, shown in Fig. 3, is similar to the one discussed above, with laser energy deposition into the thermal energy of the electrons, fast energy transfer from the electrons to the lattice due to the electron–phonon coupling, transfer of a portion of the deposited energy to the non-thermal energy associated with a stress wave and static laser-induced stresses, as well as heat conduction to the deeper part of the target represented at a continuum level. Two important distinctions, however, are (1) the presence of an additional channel of energy transfer to the latent heat of melting and (2) a significantly larger fraction of the total deposited energy transferred into the non-thermal energy of collective atomic motions and static lattice distortions.

An additional line associated with a transient melting of a 61 nm region of the target is shown in Fig. 3b and c. The energy spent on melting is determined by multiplying the fraction of the liquid phase in the system at any given time by the latent heat of melting of the model material. The fraction of the liquid phase is determined based on the local order parameter, whereas the latent heat of melting is calculated for the model EAM Ni as discussed in [8]. The time dependence of the energy of melting, E_m, reflects the two-step character of the melting process discussed above. A fast homogeneous melting of ~56 nm region of the target within ~35 ps corresponds to the initial sharp increase of E_m, whereas a much slower melting of an additional ~5 nm part of the target corresponds to the slower increase of E_m that continues up to ~250 ps after the laser pulse (Fig. 3b). Epitaxial recrystallization of the melted region, that starts at ~250 ps and is completed by the time of 1300 ps, leads to a gradual transfer of the latent heat of melting to the thermal energy of the lattice (Fig. 3c). The energy release from the recrystallization process partially compensates the cooling of the surface region due to the heat conduction to the bulk of the target. With the end of recrystallization at 1300 ps, the cooling becomes faster as evidenced by the faster decrease of the energy associated with the quasi-static thermoelastic stresses, $E_a^{\text{non-th-MD}}$ (Fig. 3c).

The fraction of the laser energy transferred into non-thermal energy ($E_a^{\text{non-th-MD}}+E_{\text{wave}}$) is significantly larger in the simulation performed at 107.5 mJ/cm^2 as compared to the one performed at 21.5 mJ/cm^2. The total fraction of non-thermal energy at 107.5 mJ/cm^2 changes from ~18% at the peak of the dynamic relaxation of thermoelastic stresses at ~35 ps, to ~13% at 250 ps after the laser pulse (as compared to 10% and 5% at 21.5 mJ/cm^2). The thermoelastic wave carries away more than 5% of the deposited laser energy at 107.5 mJ/cm^2 and only ~2% at 21.5 mJ/cm^2. The energy associated with quasi-static thermoelastic stresses at 250 ps after the laser pulse is ~8% of the deposited laser energy at 107.5 mJ/cm^2 and ~3% at 21.5 mJ/cm^2.

When laser fluence exceeds the melting threshold, the energy transfer to the latent heat of melting provides an additional channel of energy redistribution. In the simulation performed at 107.5 mJ/cm^2, up to 12% of the deposited laser energy went to the latent heat of melting of a 61 nm layer of the target. As a result of energy transfer to the non-thermal energy and the latent heat of melting, the maximum fraction of the thermal energy in the top 100 nm surface region of the target, $E_a^{\text{th-MD}}$, decreases with increasing laser fluence and is 51% of the deposited laser energy at 107.5 mJ/

cm^2 and 77% at 21.5 mJ/cm^2. At higher laser fluences, additional channels of energy transfer are provided by the onset of photomechanical damage or ablation, when a large fraction of the deposited laser energy goes into potential energy of voids/defects generated in a sub-surface region or to the energy spent on material disintegration. Both photomechanical damage and ablation have been shown to result in a fast cooling of the target material [10,19].

4. Summary

The relative contributions of different laser-induced processes to the energy partitioning and redistribution in a target irradiated by a short, 1 ps, laser pulse is investigated based on the results of computer simulations performed with a combined TTM–MD model. The energy transferred from the excited electrons to the lattice splits into several parts, namely:

(1) the energy of the thermal motion of the atoms;
(2) the energy of collective atomic motions associated with the relaxation of laser-induced stresses and the energy of quasi-static anisotropic stresses;
(3) the energy carried away from the surface region of the target by a stress wave propagating deeper into the bulk of the target;
(4) at laser fluence above the melting threshold, the energy transferred to the latent heat of melting and then released upon recrystallization.

The presence of the non-thermal channels of energy redistribution, not accounted for in the conventional TTM model, can have important implications for interpretation of experimental results on the kinetics of thermal and mechanical relaxation of a target irradiated by a short laser pulse as well as on the characteristics of laser-induced phase transformations. The energy carried away from the surface region of the irradiated target by a stress wave and the energy transferred into the energy of quasi-static thermoelastic stresses are taken away from the thermal energy of atomic motions, thus reducing the temperature of the surface. At the same time, the anisotropic lattice distortions associated with quasi-static thermoelastic stresses can significantly reduce the lattice stability against the initiation of melting [9,13] and, possibly, can induce solid-state phase transformations [20]. The fraction of the non-thermal energy in the total laser energy partitioning increases with increasing laser fluence.

Acknowledgements

Financial support of this work is provided by the National Science Foundation through the Thermal Transport and Thermal Processes Program of the Chemical and Transport Systems Division (CTS-0348503).

References

[1] S.I. Anisimov, B.L. Kapeliovich, T.L. Perel'man, Sov. Phys. JETP 39 (1974) 375.
[2] J. Hohlfeld, S.-S. Wellershoff, J. Güdde, U. Conrad, V. Jähnke, E. Matthias, Chem. Phys. 251 (2000) 237.
[3] G.L. Eesley, Phys. Rev. B 33 (1986) 2144.
[4] P.J. Antaki, Int. J. Heat Mass Transfer 45 (2002) 4063.
[5] P.M. Norris, A.P. Caffrey, R.J. Stevens, J.M. Klopf, J.T. McLeskey Jr., A.N. Smith, Rev. Sci. Instrum. 74 (2003) 400.
[6] J.K. Chen, J.E. Beraun, Numer. Heat. Transfer A Appl. 40 (2000) 1.
[7] J.K. Chen, J.E. Beraun, L.E. Grimes, D.Y. Tzou, Int. J. Solids Struct. 39 (2002) 3199.
[8] D.S. Ivanov, L.V. Zhigilei, Phys. Rev. B 68 (2003) 064114.
[9] D.S. Ivanov, L.V. Zhigilei, Phys. Rev. Lett. 91 (2003) 105701.
[10] E. Leveugle, D.S. Ivanov, L.V. Zhigilei, Appl. Phys. A 79 (2004) 1643.
[11] C. Schäfer, H.M. Urbassek, L.V. Zhigilei, Phys. Rev. B 66 (2002) 115404.
[12] D.S. Ivanov, L.V. Zhigilei, Appl. Phys. A 79 (2004) 977.
[13] L.V. Zhigilei, D.S. Ivanov, E. Leveugle, B. Sadigh, E.M. Bringa, Proc. SPIE 5448 (2004) 505.
[14] L.V. Zhigilei, B.J. Garrison, Mater. Res. Soc. Symp. Proc. 538 (1999) 491.
[15] C. Schäfer, H.M. Urbassek, L.V. Zhigilei, B.J. Garrison, Comput. Mater. Sci. 24 (2002) 421.
[16] X.W. Zhou, H.N.G. Wadley, R.A. Johnson, D.J. Larson, N. Tabat, A. Cerezo, A.K. Petford-Long, G.D.W. Smith, P.H. Clifton, R.L. Martens, T.F. Kelly, Acta Mater. 49 (2001) 4005.
[17] K. Sokolowski-Tinten, J. Bialkowski, M. Boing, A. Cavalleri, D. von der Linde, Phys. Rev. B 58 (1998) R11805.
[18] L.D. Landau, E.M. Lifshitz, Mechanics, third ed. Pergamon Press, Oxford, New York, 1976.
[19] L.V. Zhigilei, B.J. Garrison, J. Appl. Phys. 88 (2000) 1281.
[20] S.I. Anisimov, V.V. Zhakhovskii, N.A. Inogamov, K. Nishihara, A.M. Oparin, Yu.V. Petrov, Pis'ma Zh. Eksp. Teor. Fiz. 77 (2003) 731 (JETP Lett. 77 (2003) 606).